JACS
JOURNAL OF THE AMERICAN CHEMICAL SOCIETY

Article

pubs.acs.org/JACS

Mn^{2+}-Doped Lead Halide Perovskite Nanocrystals with Dual-Color Emission Controlled by Halide Content

Wenyong Liu, Qianglu Lin, Hongbo Li, Kaifeng Wu, István Robel, Jeffrey M. Pietryga, and Victor I. Klimov*

Chemistry Division, Los Alamos National Laboratory, Los Alamos, New Mexico 87545, United States

Supporting Information

ABSTRACT: Impurity doping has been widely used to endow semiconductor nanocrystals with novel optical, electronic, and magnetic functionalities. Here, we introduce a new family of doped NCs offering unique insights into the chemical mechanism of doping, as well as into the fundamental interactions between the dopant and the semiconductor host. Specifically, by elucidating the role of relative bond strengths within the precursor and the host lattice, we develop an effective approach for incorporating manganese (Mn) ions into nanocrystals of lead-halide perovskites ($CsPbX_3$, where X = Cl, Br, or I). In a key enabling step not possible in, for example, II–VI nanocrystals, we use gentle chemical means to finely and reversibly tune the nanocrystal band gap over a wide range of energies (1.8–3.1 eV) via postsynthetic anion exchange. We observe a dramatic effect of halide identity on relative intensities of intrinsic band-edge and Mn emission bands, which we ascribe to the influence of the energy difference between the corresponding transitions on the characteristics of energy transfer between the Mn ion and the semiconductor host.

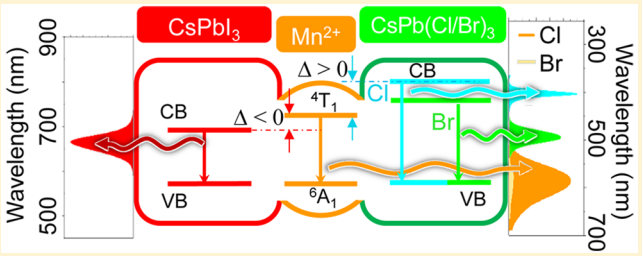

INTRODUCTION

Lead halide perovskites have attracted a great deal of attention as active materials for the realization of high-efficiency solar cells,[1−4] color-tunable light-emitting diodes (LEDs),[5] and lasers.[6,7] More recently, nanostructures, especially nanocrystals (NCs) of the hybrid perovskite[8] $(CH_3NH_3)PbX_3$[9] and the all-inorganic perovskite $CsPbX_3$ (X = Cl, Br, or I),[10] have been shown to exhibit narrow, highly efficient photoluminescence (PL) tunable over the entire visible spectral range by control over NC size and anion identity. Intriguingly, it has been shown that due to the high mobility of anions in the relatively open perovskite crystal structure,[11] halide exchange can be used to tune the NC composition postsynthetically under mild conditions, allowing very fine control of the $CsPbX_3$ NC band gap while retaining both NC morphology and high PL quantum yield (QY).[12,13] This tunability gives $CsPbX_3$ NCs unique advantages over other NC materials for use in color-selectable narrow-line-width LEDs[14,15] and low-threshold lasers based on single-[16,17] and multiphoton[18,19] pumping.

An additional level of control over the electronic and optical properties of NCs can, in principle, be afforded by the incorporation of impurity ions. Impurity doping has been demonstrated as a means of introducing novel functionalities into more traditional II–VI and III–V NCs where it is used to impart *p*- and *n*-type behaviors,[20] magnetism,[21−27] and impurity-based PL,[28,29] in some cases coexisting with band-edge PL, resulting in two-color emission.[30,31] The most commonly used impurity dopants to date are Mn^{2+},[21,22,32−38] Cu^{2+},[28,29,39] Ag^{+},[20,40] and Co^{2+}.[26,41,42] Doping of II–VI semiconductor NCs with Mn^{2+} has been particularly widely studied[21,22,32−36,38] because it potentially imparts both novel magnetic and optical properties. Due to strong exchange interactions of the 5/2 Mn^{2+} spin with conduction- and valence-band carriers, incorporation of manganese into the crystal lattice imparts paramagnetism to II–VI materials including ZnSe,[21] ZnS,[43] CdS,[36] and CdSe,[26] in both bulk[44] and nanocrystalline[45] forms, which is clearly manifested at cryogenic temperatures. At the same time, it also introduces a new emission channel at ~2.15 eV, due to an internal $^4T_1$ to $^6A_1$ transition of the Mn ion, which is largely insensitive to the exact physical and electronic structure of the host material, including the presence of electronic traps. This nominally forbidden transition is activated by impact excitation[46,47] from the optically excited carrier of the NC host to the dopant ion, resulting in relatively efficient emission with extremely long relaxation time constants (ca. 1 ms).[48,49] The time inverse of impact excitation, that is, Auger recombination, has also been demonstrated as a de-excitation pathway of the dopant ions under electrochemically controlled charging conditions;[50] however, in most circumstances radiative recombination of the excited ions is the dominant relaxation mechanism. The extended excited-state lifetimes have made such Mn^{2+}-doped NCs useful for sensitized mesoporous titania solar cells[51] and phosphorescence biosensing.[52] Moreover, because of the essentially fixed energy of dopant emission, a large, tunable

Received: August 3, 2016
Published: October 19, 2016

DOI: 10.1021/jacs.6b08085
J. Am. Chem. Soc. 2016, 138, 14954−14961

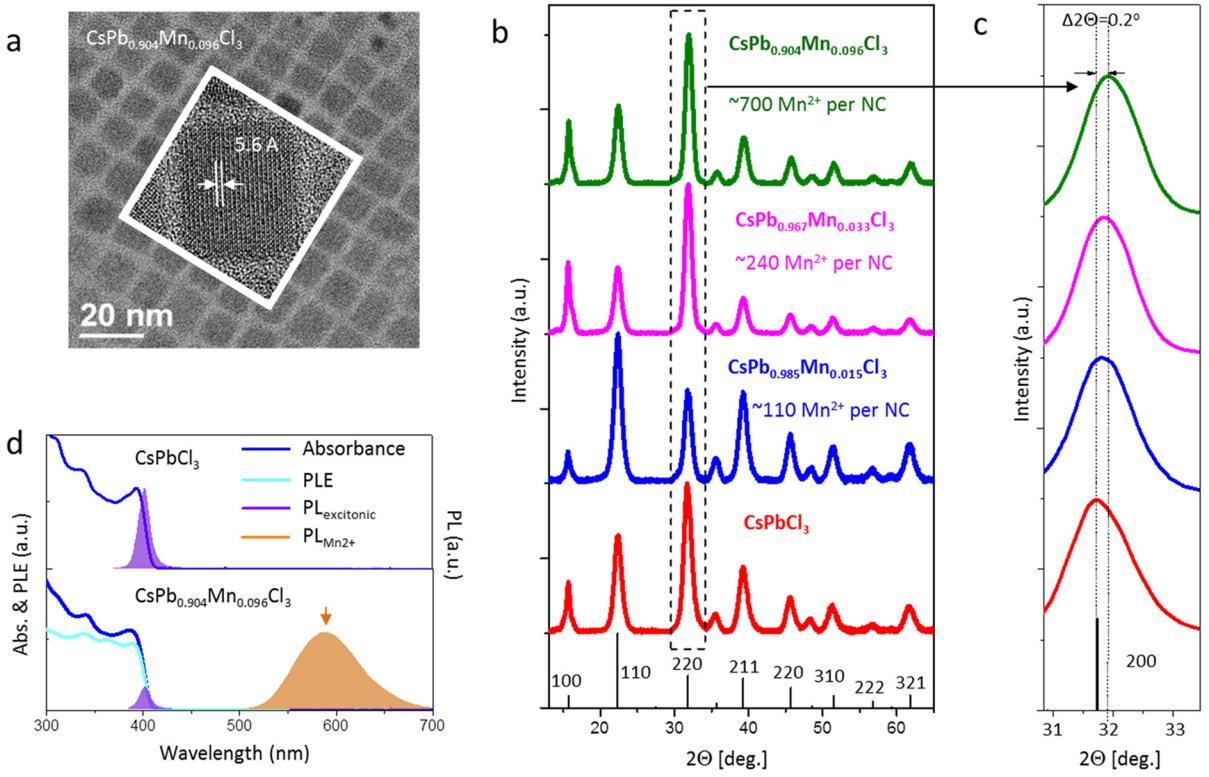

Figure 1. Morphological, spectral, and structural characterizations of undoped and Mn-doped $CsPbCl_3$ NCs. (a) TEM and (inset) HRTEM of Mn-doped $CsPbCl_3$ NCs. The distance between lattice planes in the HRTEM image is 5.6 Å, consistent with that expected along the (100) direction of the cubic perovskite structure. (b) XRD patterns of $CsPbCl_3$ NCs with different doping concentrations (according to elemental analysis by ICP-AES) showing that the cubic structure is preserved after Mn-doping. The estimated number of Mn^{2+} ions is based on a cube-shaped NC with side length of 11 nm. (c) A subtle yet monotonic shift of the (200) XRD peak toward higher 2θ is the result of progressive lattice contraction as the concentration of Mn^{2+} ions increases, as expected for substitutional replacement of Pb^{2+} ions with isovalent yet smaller Mn^{2+} ions. See Supporting Information for a detailed analysis of the significance of this shift. (d) The optical properties of undoped (top) and Mn-doped (bottom) $CsPbCl_3$ NCs. The absorption and PL spectra of undoped NCs are consistent with those from previous reports.[10,12] Doped NCs exhibit dual-color emission, with the broad peak at ~586 nm arising from a Mn^{2+} d−d transition. The PLE spectrum for the Mn^{2+} emission peak resembles the absorption spectrum, indicating that it is sensitized by the host NC.

Stokes shift can be realized by modifying the size or composition of the host NC, which is of benefit for luminescent solar concentrators[53] and multiphoton biomedical imaging.[54]

In some cases, a Mn-related PL band was reported to be observed simultaneously with intrinsic band-edge emission,[21] which was initially interpreted in terms of coexisting subensembles of doped and undoped NCs. However, follow-up investigations of dual-band PL have revealed a clear dependence of the relative intensities of the two bands on the energy difference of the corresponding optical transitions, suggesting that both PL features originate from doped NCs.[30] The properties of dual-band emission have been typically probed in Mn^{2+}-doped II−VI NCs and nanoheterostructures[23] through size-tuning of the host band gap using quantum confinement effects. Reported methods for accomplishing this present complications, because they involve prolonged heating at high temperatures that can cause loss of dopants or poorly controlled particle growth.[34] In contrast, using $CsPbX_3$ NCs one has the ability to flexibly *and reversibly* change the band gap energy via anion (halide) exchange at very mild conditions that preserve the cation sublattice and NC dimensions.[12,13]

Here, we introduce a facile synthetic approach for producing Mn^{2+}-doped $CsPbX_3$ (Mn:$CsPbX_3$) NCs with finely tunable anion content. This is accomplished by directly synthesizing Mn:$CsPbCl_3$ NCs, followed by anion exchange to create NCs of Mn:$CsPbBr_3$, Mn:$CsPbI_3$, and those of mixed anion content. In this approach, the host energy gap (E_g) can be continuously and reversibly varied, after doping, over the range from 1.8 to 3.1 eV, which covers energies both below and above the Mn^{2+} d−d transition (E_{Mn} = 2.15 eV) while preserving NC size and shape. These NCs represent a truly unique testbed for the study of host−dopant interactions, as well as a versatile material class for the development of technologies that can exploit tunable Stokes shift or dual-color emission.

RESULTS

Synthesis and Microstructural Characterization of Doped NCs. Mn-doped $CsPbCl_3$ NCs were prepared using a modified version of a previously reported synthesis of undoped NCs[10] in which a source of Mn is introduced into the reaction mixture. As described in greater detail below, after testing several possible Mn-precursors, we found $MnCl_2$ allowed for facile control of Mn-content in the product NCs. In a typical reaction, $PbCl_2$ and $MnCl_2$ were dissolved in a mixture of octadecene, trioctylphosphine, oleylamine, and oleic acid under vacuum at 100 °C; nucleation and growth of particles was then initiated by the swift injection of a cesium oleate stock solution at 185 °C (see Supporting Information for details). NCs were collected from the growth solution by centrifugation and redispersion in hexane.

DOI: 10.1021/jacs.6b08085
J. Am. Chem. Soc. 2016, 138, 14954−14961

The as-prepared NCs show a cubic morphology with the average side length of ~11 ± 1.0 nm (Figure 1a, Supporting Figures S1–S3), similar to the undoped ones (Supporting Figure S4). Both high-resolution transmission electron microscopy (HRTEM, Figure 1a, inset) and powder X-ray diffraction (XRD, Figure 1b) demonstrate that the NCs are highly crystalline. By variation of the Pb/Mn stoichiometry during the reaction, different concentrations of dopant can be achieved in the product NCs. As shown in Figure 1c, NCs with various dopant concentrations [as determined by inductively coupled plasma atomic emission spectroscopy (ICP-AES)] have XRD patterns structurally identical to the undoped NCs.[10] Careful examination of the XRD patterns reveals that the peaks are monotonically shifted to higher angles with increasing dopant concentration, as demonstrated for the (200) peak in Figure 1c. This is consistent with lattice contraction due to the substitution of Pb^{2+} ions (six-coordinate crystal ionic radius 133 pm) with smaller Mn^{2+} ions (97 pm).[55] Despite the significant difference in cation size, doped NCs are observed to have stability much the same as undoped NCs. Both NCs retain their crystal structures for at least several months, and are relatively stable in air, although sensitive to moisture.

Undoped NCs exhibit absorption and PL features consistent with previous reports,[10] including narrow band-edge emission [full-width at half-maximum (fwhm) of ca. 110 meV] at 402 nm (Figure 1d, top). The band-edge spectral features of doped NCs are very similar in appearance but are joined by an additional broad PL band (fwhm ca. 200 meV) attributable to Mn^{2+} d–d emission, which peaks at ~586 nm (Figure 1d, bottom) independent of dopant concentration.[44] The internal Mn^{2+} transition is universally broad in doped II–VI systems in both bulk and nanostructure morphologies.[44,56] Importantly, the PL excitation (PLE) spectrum collected by monitoring the PL at 586 nm closely follows the absorption spectrum (Figure 1d, bottom), implying that just as in Mn-doped II–VI NCs,[21] the nominally forbidden Mn^{2+} emission is sensitized by the $CsPbCl_3$ NC host, unambiguously demonstrating the success of Mn^{2+} doping.

The as-prepared undoped $CsPbCl_3$ NCs tend to have relatively low PL QY (<5%), as previously observed.[12,13] As shown in Figure 2a, while doped NCs exhibit similar band-edge emission QYs regardless of Mn concentration, the PL QY of Mn^{2+} transition increased proportionately with the doping level, up to a maximum of 27% for NCs containing 9.6% Mn (relative to Pb), leading to an overall yellow-orange color of the emission (Figure 2b). Attempted incorporation of still larger amounts of Mn produces a product with qualitatively identical spectral features but with dramatically lower QY for both band-edge and dopant emission, implying that it comprises NCs with surface or internal defects, possibly combined with other reaction side-products. Closer inspection reveals that both the band-edge absorption and PL peaks of Mn:$CsPbCl_3$ NCs shift very slightly yet continuously to the blue as Mn-concentration increases (Figure 2c,d), despite no apparent change in NC size. This phenomenon is similar to that observed in Mn^{2+}-doped CdSe NCs,[34] in which it was attributed to effects of Mn-alloying on the band gap of the host material itself. Similar effects are likely involved in Mn:$CsPbCl_3$ NCs; the broadening of the band-edge absorption feature, then, reflects the statistical variation of the number of Mn^{2+} ions doped into individual NCs within the ensemble of a given average composition.

Effect of Identity of Mn Precursor. As with incorporation of Mn^{2+} into II–VI NCs during growth,[57] doping into lead

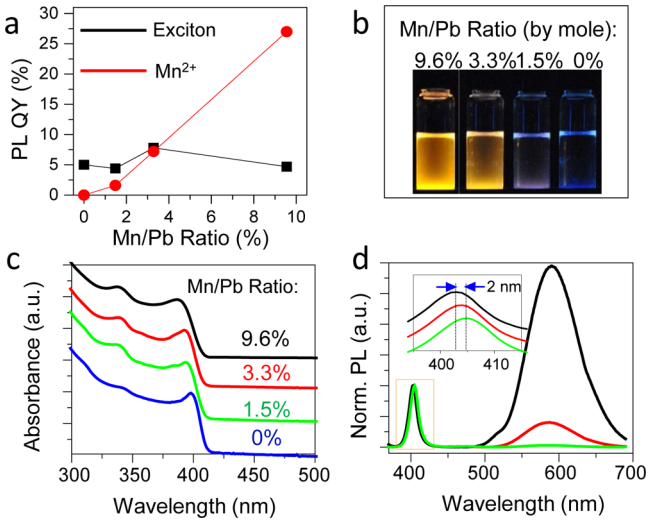

Figure 2. The dependence of Mn:$CsPbCl_3$ NC optical properties on dopant concentration. (a) While the absolute PL QY of the band-edge emission is largely independent of dopant concentration, the PL QY of the Mn^{2+} d–d transition depends on it directly. (b) Photograph of hexane solutions of Mn:$CsPbCl_3$ NCs of varying Mn-content illuminated by a UV lamp (365 nm). Solutions were diluted to exhibit the same optical density at 365 nm. The UV emission of the host NC is essentially invisible, while the orange Mn-based emission grows in intensity with dopant concentration. (c) Normalized absorption and (d) PL spectra of Mn:$CsPbCl_3$ NCs of varying dopant concentration. Increased Mn-content is associated with a gradual blue-shift of both the band-edge peak in absorption and the intrinsic NC PL peak [expanded in the inset of panel d]; this can be attributed to the effects of alloying on the NC band structure. The Mn-emission peak grows in intensity with increasing Mn-content but does not shift.

chloride perovskite NCs does not seem to be driven by thermodynamic equilibrium forces but instead reflects the influence of reaction kinetics, wherein among other factors, the identity of the dopant precursor plays a vital role. Evidence for this is drawn from a series of doping experiments using a variety of manganese halides and carboxylates. As demonstrated above, Mn:$CsPbCl_3$ NCs with various doping concentrations can be readily obtained with $MnCl_2$ as the precursor. In fact, it is so effective that 0.2% (by mole) of this compound in the reaction mixture can lead to the appearance of Mn^{2+} emission. In contrast, no evidence of doping was observed when carboxylates such as $Mn(ac)_2$, $Mn(acac)_2$, and $Mn(oleate)_2$ were used. From this, we might infer that the preexisting Mn–Cl bond is beneficial for incorporation of Mn into the lattice of the growing NC, where the Pb (or Mn) site features an all-Cl coordination sphere. The use of precursors with preexisting bonds to the desired anion has been found to help with incorporation of dopants in II–VI NCs.[26,41] In contrast, the strong Mn–O bond in the carboxylate precursors raises a barrier to inclusion, potentially due to both the thermodynamic cost of breaking the bond and the disruption to lattice formation imposed by any remaining carboxylate ligands.

Although the simplicity of this model is attractive, attempts with Br^- and I^- containing NCs suggest more subtle factors are at play. The addition of $MnBr_2$ as the doping precursor during synthesis of $CsPbBr_3$ does not result in the characteristic Mn^{2+} d–d emission in product NCs; the absence of Mn is further corroborated by ICP-AES elemental analysis. Likewise, no trace of Mn is found according to ICP-AES of $CsPbI_3$ NCs after attempted doping with MnI_2 [Mn^{2+} emission is not expected in

DOI: 10.1021/jacs.6b08085
J. Am. Chem. Soc. 2016, 138, 14954–14961

this case, since the band gap of the host material (1.73 eV) is smaller than that of the Mn^{2+} d−d transition]. In light of these findings, we suggest that the success of using $MnCl_2$ as a dopant can be attributed to the similarity of bond strengths within the precursor and the growing lattice, rather than to any specific common ion effects (see Discussion section).

Doping of Hybrid Perovskite NCs. To test the applicability of this approach to similar systems, the full series of common and mixed halide reactions were attempted using $(CH_3NH_3)Cl$ in place of cesium oleate, so as to produce Mn-doped NCs of the hybrid perovskite $(CH_3NH_3)PbX_3$. The results were qualitatively identical, with prominent Mn-based PL peaks observed for $PbCl_2/MnCl_2$ reactions (Supplementary Figure S5).

Postsynthetic Halide Exchange. Recently, reversible halide exchange under mild reaction conditions has been reported in the literature for perovskites of various morphologies including films,[58] NCs,[12,13] and nanoplatelets.[59] In NCs, control over the amount of the injected halide precursor has been shown to yield a predictable halide ratio in the product NCs, allowing one to finely tune the band gap. This is an especially intriguing possibility in the case of doped perovskite NCs, wherein the relative intensities of the host and Mn^{2+} emission bands should depend on the energy difference between the NC band gap and the fixed energy of the Mn^{2+} transition.

We indeed found that Mn-doped $CsPbBr_3$ and $CsPbI_3$ NCs, as well as NCs of mixed halide composition, could be obtained by performing anion exchange on Mn:$CsPbCl_3$ NCs. To start with, we prepared Mn:$CsPbCl_3$ NCs and reacted them with $PbBr_2$ as a bromide precursor to produce a series of Mn:$CsPbCl_xBr_{3-x}$ NCs. During this process, the morphology and the crystal structure are preserved (Supplementary Figure S6a,b), as in the case of undoped NCs.[12,13] As increasing amounts of bromide precursor are added, the band-edge PL peak shifts monotonically to the red, eventually reaching 2.49 eV, near the previously reported PL peak energy of pure $CsPbBr_3$ NCs (2.43 eV),[12] while the Mn^{2+} emission, as an internal transition, stays constant in energy throughout the exchange (Figure 3a). Upon treatment of these Mn:$CsPbBr_3$ NCs with PbI_2 (Supplementary Figure S6c), the band-edge PL shifts further to the red (Supplementary Table S1); eventually its energy becomes smaller than that of the Mn transition, at which point there is no longer any trace of Mn-based emission (Supplementary Figure S7).

As anion exchange is performed, dramatic changes in the intensities of both the band-edge and dopant emission are observed. The first small amounts of bromide produce a significant increase in the QY of both peaks (Supplementary Figure S8). During subsequent addition, the QY of the band-edge peak continues to grow until it stabilizes at a value typically as high as 80%. In contrast, after the initial spike, the PL QY of the Mn^{2+} transition slowly declines, ultimately reaching <5% (Supplementary Figure S8). The net result is that after some fluctuation in the region in which the intensity of both peaks changes rapidly, the ratio of the Mn-to-band-edge PL QY monotonically decreases with increasing Br^- content (Figure 3a and Supplementary Figure S9a). This might imply the loss of Mn during the anion exchange reaction; however, we observe that this trend is reversible. Specifically, applying a reverse halide exchange from Br^- to Cl^- to the same NC sample using $PbCl_2$ as the precursor (Figure 3b and Supplementary Figure S9b) causes the band-edge peak to blue-shift back to its original position. This is accompanied by a restoration of the amplitude of the Mn PL peak, which virtually retraces the changes observed during the direct Cl-to-Br anion exchange (Figure 3c). While the recovery of the Mn emission is not complete (see analysis below in Discussion section), it is clear that the evolution of the PL spectra is not due to changes in Mn content and is instead a function of changes in the branching ratio between the two emission channels occurring as a result of the change in the band-edge transition energy. Specifically, the closer E_g is to E_{Mn}, the greater the relative intensity of the band-edge PL compared to the intensity of the Mn PL peak.

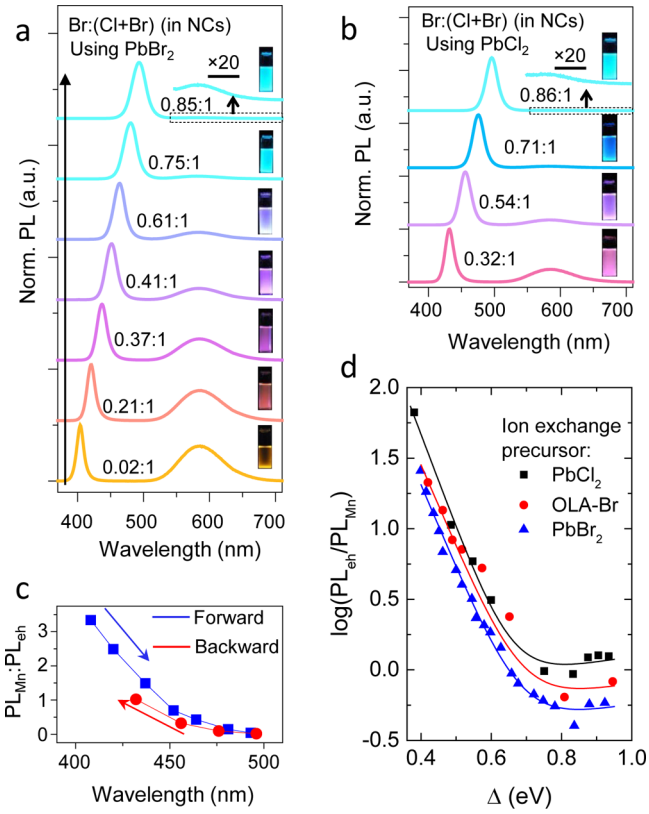

Figure 3. The evolution of Mn:$CsPbCl_{3-x}Br_x$ NCs PL energy and intensity during anion exchange. (a) PL spectra of NC samples taken during progressive Br^- anion exchange using $PbBr_2$, starting with $CsPbCl_3$ NCs (bottom). Spectra are normalized at the peak of the band-edge (shorter-wavelength) emission feature. The expected gradual red shift of the band-edge emission was accompanied by a suppression of Mn-emission. (b) PL spectra of NC samples during the reverse anion exchange reaction, starting at the top with the most Br-rich sample from panel a, using $PbCl_2$. As Br-content decreases, the band-edge peak blue-shifts and the intensity of the Mn-emission recovers. (c) The dependence of the ratio of the PL QY of the Mn- and band-edge-emissions (PL_{Mn}/PL_{eh}) on band edge PL wavelength during both the forward (blue) and reverse (red) anion exchange reactions. The incomplete recovery of Mn^{2+} PL intensity during the reverse reaction reveals some amount of Mn^{2+} loss through cation exchange with excess Pb^{2+} from the Pb-halide precursor. (d) Dependence of the PL_{eh}/PL_{Mn} ratio on the difference between the band gap and Mn^{2+} transition energies. Ion exchange is accomplished using $PbCl_2$ (black squares), OLA-Br (red circles), or $PbBr_2$ (blue triangles) as precursors. Solid lines with corresponding colors are fits based on an energy transfer model (eq 1) relating the intensities of the two transitions to their energy difference.

DOI: 10.1021/jacs.6b08085
J. Am. Chem. Soc. 2016, 138, 14954−14961

DISCUSSION

Doping of Mn^{2+} into II−VI semiconductor NCs has been demonstrated to be much more difficult than doping of corresponding bulk materials. This is because for NCs, the proximity of all lattice sites to the surface means that thermal equilibrium between the impurity reservoir in solution and the dopants included within the NC favors exclusion. Indeed, at typical colloidal synthesis temperatures (<350 °C), the impurity diffusion rate into the semiconductor lattice is negligible.[57] Therefore, doping is accomplished via control over kinetic factors. In one example of this, Erwin et al.[57] proposed that impurity incorporation can be affected by taking advantage of strong binding of dopant ions to specific crystal facets, followed by material overgrowth. Alternatively, doping has also been achieved by using polychalcogenide precursors, which feature Mn directly bound to other lattice constituents in cluster form, favoring inclusion.[41,60] This latter case is not unlike what we observe in the synthesis of Mn:$CsPbCl_3$ NCs, in which the pre-existing Mn−Cl bond of the $MnCl_2$ precursor seems to favor Mn incorporation.

As mentioned in Results, this approach does not work for doping $CsPbBr_3$ and $CsPbI_3$. To explain this disparity, we examine the potential role of bond strengths within the precursor and growing lattice, using the energy of homolytic dissociation of diatomic molecules for the sake of these comparisons. In the most successful doping example, the bond dissociation energy of Mn−Cl (338 kJ/mol)[61,62] is only slightly higher (by 12%) than that of Pb−Cl (301 kJ/mol).[62] We suggest that the similar bond energy favors mixing of these isovalent ions within the lattice, leading to the successful doping. In contrast, the energy difference is much larger for the other two cases. For instance, the Mn−Br (314 kJ/mol)[61,62] bond is stronger than the Pb−Br bond (249 kJ/mol)[62] by 26% and the bond energy of Mn−I (282 kJ/mol)[61,62] is fully 46% greater than that of Pb−I (194 kJ/mol).[62] This large disparity in bond energies is likely to favor extended domains of MnX_2 over a dispersion of Mn^{2+} within the perovskite lattice, preventing formation of doped NCs. This correlation between precursor bond strengths and doping success suggests that precursor decomposition is an important step in the NC formation reaction. This finding provides a simplifying yet useful guide for the identification of other potential doping precursors, perhaps even for other impurity metals. However, a more quantitative assessment of the precise impact of precursor bond strength would require consideration of other energetic contributions, including those of solvation.

As a means for validating this model, we attempted the doping of $CsPbCl_3$ NCs with $MnBr_2$ as the manganese precursor, noting that the bond energy difference between Pb−Cl and Mn−Br is a mere 13 kJ/mol (~4%), suggesting that doping should occur. Indeed, as shown in Supporting Figure S10a−c, the NCs produced by this reaction evince the dual-color PL indicative of Mn-doping. Interestingly, the band edge emission for these NCs is red-shifted from that of pure Mn:$CsPbCl_3$ NCs, indicating the formation of mixed halide Mn:$CsPbCl_xBr_{3-x}$ perovskite NCs, and in turn implying the retention of at least some Mn−Br bonds during incorporation. The highest achievable doping concentration via this mixed anion reaction is significantly lower (ca. 0.1%, corresponding to 10 Mn^{2+} ions per NC on average; Supporting Table S2) than in the fully chloride case. This may indicate that halide exchange occurs between $PbCl_2$ and $MnBr_2$ precursors in solution, leading to the formation of $PbBr_2$ and $MnCl_2$, a reactant pair that does not favor formation of a doped product. Very similar results were produced in the synthesis of Mn:$CH_3NH_3PbBr_xCl_{3-x}$ hybrid perovskite NCs using $PbCl_2/MnBr_2$ reaction mixtures (Supplementary Figure S10d−f).

Thus, postsynthetic anion exchange of Mn:$CsPbCl_3$ is the best way to achieve doped NCs of other halide content, which offers the added advantage of reversibility. It is important to note that during the process of reverse anion exchange from Mn:$CsPbBr_3$ to Mn:$CsPbCl_3$, the recovery of Mn-emission intensity relative to that of the band-edge transition is not quantitative (Figure 3b,c). Given the relation between dopant concentration and dopant-related PL QY, this suggests some loss of Mn^{2+} during the halide exchange reactions. By comparing the Mn-to-band-edge PL QY ratio for the lowest Br-content samples during both forward and the subsequent reverse exchange reaction (Supplementary Figure S9a,b), we see a drop in Mn emission consistent with a ca. 50% reduction in Mn content. We attempted to verify this using elemental analysis by ICP-AES to determine the Mn^{2+} to Pb^{2+} ratio of samples during the forward and reverse exchange (Supplementary Table S3). These measurements largely corroborate the loss of Mn, implying some amount of cation exchange of Pb^{2+} for Mn^{2+} that may happen continuously throughout both exchange processes. However, while the ultimate Mn/Pb ratio is only 9% of that measured before the exchange cycle, the PL QY ratio (Mn/band edge) is still fully 50% of the original, suggesting that the elemental analysis is influenced by additional Pb^{2+} ions bound to the NC surface because of the extremely Pb-rich exchange reaction conditions. By the arguments offered above for achieving successful Mn-doping, it seems likely that the loss of Mn should also be affected by precursor versus lattice bond energy. In support of this, we note that the continued halide exchange of the product Mn:$CsPbBr_3$ using PbI_2 to produce Mn:$CsPbI_3$ proceeds with negligible loss of Mn, as does the direct reverse exchange of Mn:$CsPbI_3$ back into Mn:$CsPbCl_3$ using $PbCl_2$ (see Supplementary Table S1); this is likely a direct result of large energy differences between the lead−halide bonds of the anion exchange precursors and the manganese−halide bonds of the lattice in each case.

By extension, this model predicts that halide exchange using alternative, Pb-free precursors should proceed with no loss of Mn. Indeed, we find that oleylamine bromide (OLA-Br) can be used to convert Mn:$CsPbCl_3$ into Mn:$CsPbBr_3$ with quantitative retention of Mn^{2+} according to ICP-AES (see Supplementary Table S4). Unfortunately, so far the usage of OLA-X tends to lead to irreversible loss of the dispersibility of NCs, possibly due to a change in the surface stoichiometry of the NCs toward excess halide content, making it impossible to perform sequential exchanges. Nonetheless, in a forward Cl^- to Br^- exchange experiment, the use of OLA-Br results in the same pattern of changes in peak energy and intensity (Supplementary Figure S9c) as that observed for $PbBr_2$ (Supplementary Figure S9a), confirming that the reduction of the Mn-PL intensity relative to the intensity of the band-edge PL with increasing Br content occurs even when Mn is fully retained.

The dependence of the QY of the band-edge emission on halide content is in agreement with our own prior observations,[63] as well as those in other reports,[12] indicating that undoped $CsPbBr_3$ NCs generally exhibit higher emission QY than $CsPbCl_3$ NCs. We suggest that the opposite dependence of the PL intensity due to the Mn^{2+} transition,

DOI: 10.1021/jacs.6b08085
J. Am. Chem. Soc. 2016, 138, 14954−14961

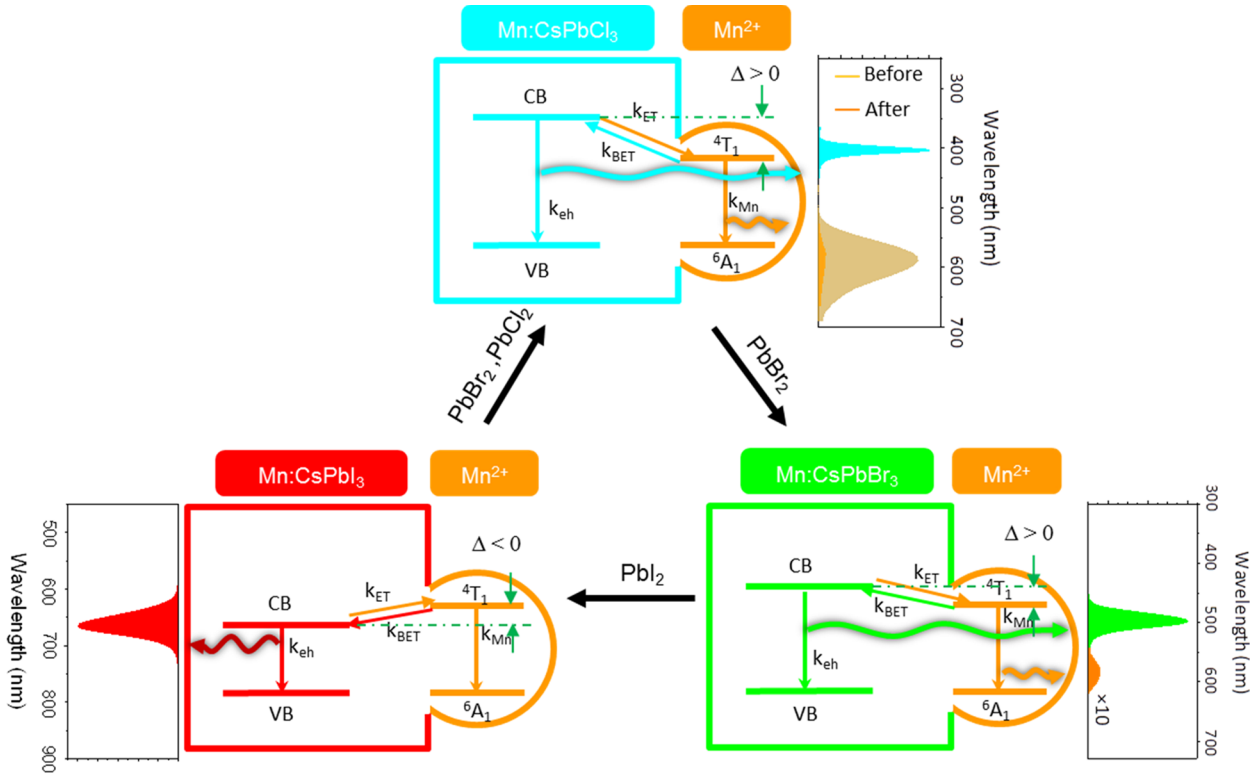

Figure 4. The evolution of the energy level diagram of Mn:$CsPbX_3$ NCs during forward and reverse anion exchange; CB and VB denote the conduction and the valence band of the NC, respectively. The relative intensities of the two PL features of Mn:$CsPbX_3$ NCs is established by the interplay of rates of several competing processes, including band edge electron−hole recombination (k_{eh}) and deactivation of the Mn^{2+}-based d−d transition (k_{Mn}), as well as forward (k_{ET}) and back (k_{BET}) energy transfer between the NC and the impurity. The competition between the latter two processes is also strongly influenced by the energy difference, Δ, between the band edge and Mn^{2+}-based transitions. In freshly prepared Mn:$CsPbCl_3$ NCs, Δ is large and positive, favoring forward energy transfer and strong Mn^{2+}-based PL (spectrum shown by yellow shading). After anion exchange with $PbBr_2$, in the resulting Mn:$CsPbBr_3$ NCs, Δ is still positive, but much smaller; in addition, some Mn^{2+} is lost to ion exchange with Pb^{2+}. Both effects lead to reduced Mn^{2+}-based PL (spectrum shown by orange shading; amplitude multiplied by a factor of 10). Further exchange with PbI_2 produces Mn:$CsPbI_3$ NCs, in which Δ is negative, resulting in no Mn^{2+}-based PL. Finally, reverse anion exchange to return to Mn:$CsPbCl_3$ NCs restores the large, positive Δ, which leads to re-emergence of Mn^{2+}-based PL; the intensity of the impurity band; however, is diminished (spectrum shown by orange shading) due to the loss of Mn^{2+} when Pb-containing exchange precursors are used.

that is, its decrease with increasing Br content (Figure 3a,b; Supplementary Figures S9a−c), is the result of the band gap-dependent redistribution of the photogenerated excitons between the band-edge and Mn-related emission channels (Figure 4). Ideally, in the absence of nonradiative processes, the ratio of the PL intensities for these channels reflects the balance between the corresponding radiative decay rates and the rates of direct and back energy transfer between the semiconductor host and Mn^{2+} ions. The forward band edge-to-Mn^{2+} energy transfer and the reverse process (Mn^{2+}-to-band edge transfer) are inherently related, and the balance between them is established principally by the energy difference (Δ) between the two transitions. The forward transfer is energetically favorable, while the back transfer is unfavorable and therefore requires thermal activation. This mechanism was previously used to elucidate the dual color emission in the ZnMnSe/CdSe system.[30] Quantitatively, the QY ratio can be expressed as[30]

$$\frac{PL_{Mn}}{PL_{eh}} = \frac{k_{Mn,rad}}{k_{eh,rad}} \frac{k_{ET}}{k_{Mn} + k_{ET}\, e^{-\alpha\Delta/kT}} \quad (1)$$

where PL_{Mn} and PL_{eh} are the experimentally measured PL intensities of the Mn^{2+} and band-edge transitions, respectively, $k_{Mn,rad}$ and $k_{eh,rad}$ are the corresponding radiative decay rate constants, k_{ET} is the rate of band edge-to-Mn^{2+} energy transfer, while the rate of back energy transfer is given by $k_{BET} = k_{ET}\exp(-\alpha\Delta/kT)$, k_{Mn} is the total de-excitation rate (radiative and nonradiative) of Mn^{2+} ions, and α is a constant of the order of unity that accounts for details of the NCs' and the Mn^{2+} ions' electronic structures, the relative positions of their energy levels, and specifics of the energy transfer process. While a rigorous physical interpretation of α is not yet available, our experimental data acquired during exchange reactions under three different sets of conditions consistently produce a narrow range of α values between 0.39 and 0.44, supporting its assignment as a materials-specific constant. When using eq 1 for data modeling, we make a simplifying assumption that $k_{Mn} = k_{Mn,rad}$, as radiative processes under normal conditions dominate Mn^{2+} de-excitation. As mentioned above, QYs and radiative rates in perovskite NCs depend on halide content; our analysis of PL spectra and dynamics in undoped $CsPbX_3$ NCs with varying halide content show a nearly monotonic increase in $k_{eh,rad}$ as the band gap increases (Supporting Figure S11). We use a linear fit to this data in eq 1 when modeling the measured intensity ratios for the band-edge and Mn^{2+} PL bands (Figure 3d).

In principle, the rates of direct and reverse energy transfer are expected to depend on the number and exact location of the Mn^{2+} ions. During the halide exchange, however, these parameters do not change as the cation sublattice (including

DOI: 10.1021/jacs.6b08085
J. Am. Chem. Soc. 2016, 138, 14954−14961

incorporated Mn^{2+} ions) seems to remain largely undisturbed. Under these conditions, we expect that the principal parameter affecting the ratio of the band-edge and Mn PL intensities is the difference between transition energies Δ. This is truly a unique situation, which is difficult to realize with other approaches to tuning a material's band gap. Our conjecture of the dominant role of Δ in defining the PL intensity ratio is validated by the excellent agreement between our measurements (symbols) and model (solid lines) shown in Figure 3d for three different halide-exchange precursors. A subtle but consistent feature of the data sets is that the PL ratio passes through a minimum at a relatively high Δ value in the range of 0.7−0.9 eV, an effect that is captured by the model only when one accounts for the band gap dependence of $k_{eh,rad}$ (see Supporting Figure S11). Depending on halide precursor, the k_{ET}/k_{Mn} ratio determined from the fits is in the $(35-82) \times 10^3$ range, yielding energy transfer lifetimes of 3−8 ns based on a literature value of $k_{Mn} = 3.7 \times 10^3\ s^{-1}$, observed for Mn-doped II−VI NCs.[49] This is ∼2 orders of magnitude slower than the previously estimated energy transfer rate for $Zn_{1-x}Mn_xSe$, meaning that the radiative rate of the band-edge transition is very similar to that of energy transfer to Mn. This similarity is a primary factor responsible for the unusually fast reduction in the Mn emission intensity as the thermodynamic driving force for energy transfer, Δ, decreases. The strikingly slower energy transfer rate in $Mn:CsPbX_3$ NCs suggests that the strength of interactions between the band-edge carriers and dopant electrons is reduced relative to that observed in Mn-doped II−VI NCs.[32] Previous studies have found that coupling between NC host and dopant carriers can be enhanced by quantum confinement.[64] Because of the smaller Bohr exciton radii of $CsPbX_3$[10] and the relatively large NC sizes in this study, our materials exhibit much weaker quantum confinement than in, for example, Mn-doped ZnSe NCs,[21] which may factor into the difference in energy transfer rates between the two systems.

CONCLUSIONS

Dual-emissive Mn^{2+}-doped perovskite NCs have been prepared by inclusion of appropriate Mn precursors during NC growth, where the choice of precursor is based on bond-strength considerations. This method should prove applicable to doping of other types of nanostructures such as nanoplatelets[8,65] and nanowires,[66] and even bulk perovskites. In this way, it significantly expands the toolbox of synthetic approaches to controlling functionality of these new classes of materials. Further, exploitation of the previously demonstrated facile anion exchange reactions affords the opportunity to finely and reversibly tune the band gap of these NCs in a manner impossible to achieve in the long-studied doped II−VI NCs. This should allow for substantial flexibility in the engineering of these NCs as dual-color emitters for sensing and labeling as well as for applications as down-converting phosphors and active elements of LEDs. In addition, the ability to change the halide composition without altering the cation sublattice comprising Mn ions provides a unique opportunity for systematic studies of interactions between the impurity and the semiconductor host as a function of halide content, which controls such characteristics of the NCs as the band gap energy and the radiative decay rate of band-edge excitons.

METHODS

Synthesis of Mn-Doped $CsPbCl_3$ NCs ($Mn:CsPbCl_3$). $Mn:CsPbCl_3$ NCs were prepared by injecting a Cs(oleate) stock solution into a heated and stirring solution of $PbCl_2$ and $MnCl_2$ in dry octadecene (ODE) with oleic acid (OA), oleylamine (OLA), and trioctylphosphine as surfactants. The reaction mixture was cooled by immersing the flask in cold water immediately after the injection. Due to the low solubility of the NCs in the ODE solution at room temperature, they could be separated out through precipitation, with the assistance of centrifugation. The precipitate was dissolved in toluene, and washed again by precipitating via the addition of acetonitrile, centrifugation, and redispersion in toluene. The dopant concentration was controlled by varying the ratio of the $MnCl_2$ and $PbCl_2$ precursors. Mn^{2+}-doped $CsPbCl_{1-x}Br_x$ NCs were synthesized by replacing $MnCl_2$ with $MnBr_2$ while keeping the rest of the reaction parameters the same. Detailed procedures are described in Supporting Information.

Postsynthetic Anion Exchange. The anion exchange reaction was performed at room temperature under inert atmosphere using Schlenk-line techniques. To prepare $Mn:CsPbCl_{3-x}Br_x$ NCs, the as-synthesized $Mn:CsPbCl_3$ NCs were dispersed in anhydrous hexane. A $PbBr_2$ stock solution was slowly added to a vigorously stirring NC solution. Progress in the halide exchange reaction was monitored by performing absorption and PL measurements on aliquots taken periodically during the reaction. With the addition of the Br^- precursor, a monotonic red shift of the band-edge PL was observed. In an alternative approach, $PbBr_2$ was replaced with OLA-Br, with the remaining reaction parameters left the same. After the reaction, the NCs were separated by centrifugation and redispersed in anhydrous hexane. Applying the same anion-exchange protocol, the fabricated $Mn:CsPbCl_{3-x}Br_x$ NCs could be converted into $Mn:CsPbBr_{1-x}I_x$ or $Mn:CsPbCl_3$ NCs, using PbI_2 or $PbCl_2$, respectively, as precursors.

ASSOCIATED CONTENT

Supporting Information

The Supporting Information is available free of charge on the ACS Publications website at DOI: 10.1021/jacs.6b08085.

Details of nanocrystal synthesis and characterization, additional TEM images, additional absorption and PL spectra, elemental analysis data, and radiative lifetimes of undoped $CsPbCl_{1-x}Br_x$ NCs (PDF)

AUTHOR INFORMATION

Corresponding Author

*klimov@lanl.gov

Notes

The authors declare no competing financial interest.

ACKNOWLEDGMENTS

This work was supported by the Chemical Sciences, Biosciences and Geosciences Division, Office of Basic Energy Sciences, Office of Science, U.S. Department of Energy. K.W. was supported by a Los Alamos National Laboratory Director's Fellowship.

REFERENCES

(1) Liu, M.; Johnston, M. B.; Snaith, H. J. *Nature* **2013**, *501*, 395.
(2) Shi, D.; Adinolfi, V.; Comin, R.; Yuan, M.; Alarousu, E.; Buin, A.; Chen, Y.; Hoogland, S.; Rothenberger, A.; Katsiev, K.; Losovyj, Y.; Zhang, X.; Dowben, P. A.; Mohammed, O. F.; Sargent, E. H.; Bakr, O. M. *Science* **2015**, *347*, 519.
(3) Nie, W.; Tsai, H.; Asadpour, R.; Blancon, J.-C.; Neukirch, A. J.; Gupta, G.; Crochet, J. J.; Chhowalla, M.; Tretiak, S.; Alam, M. A.; Wang, H.-L.; Mohite, A. D. *Science* **2015**, *347*, 522.
(4) Jeon, N. J.; Noh, J. H.; Yang, W. S.; Kim, Y. C.; Ryu, S.; Seo, J.; Seok, S. I. *Nature* **2015**, *517*, 476.
(5) Tan, Z.-K.; Moghaddam, R. S.; Lai, M. L.; Docampo, P.; Higler, R.; Deschler, F.; Price, M.; Sadhanala, A.; Pazos, L. M.; Credgington,

DOI: 10.1021/jacs.6b08085
J. Am. Chem. Soc. 2016, 138, 14954−14961

D.; Hanusch, F.; Bein, T.; Snaith, H. J.; Friend, R. H. *Nat. Nanotechnol.* **2014**, *9*, 687.
(6) Xing, G.; Mathews, N.; Lim, S. S.; Yantara, N.; Liu, X.; Sabba, D.; Grätzel, M.; Mhaisalkar, S.; Sum, T. C. *Nat. Mater.* **2014**, *13*, 476.
(7) Zhu, H.; Fu, Y.; Meng, F.; Wu, X.; Gong, Z.; Ding, Q.; Gustafsson, M. V.; Trinh, M. T.; Jin, S.; Zhu, X. Y. *Nat. Mater.* **2015**, *14*, 636.
(8) Sichert, J. A.; Tong, Y.; Mutz, N.; Vollmer, M.; Fischer, S.; Milowska, K. Z.; García Cortadella, R.; Nickel, B.; Cardenas-Daw, C.; Stolarczyk, J. K.; Urban, A. S.; Feldmann, J. *Nano Lett.* **2015**, *15*, 6521.
(9) Zhang, F.; Zhong, H.; Chen, C.; Wu, X.-g.; Hu, X.; Huang, H.; Han, J.; Zou, B.; Dong, Y. *ACS Nano* **2015**, *9*, 4533.
(10) Protesescu, L.; Yakunin, S.; Bodnarchuk, M. I.; Krieg, F.; Caputo, R.; Hendon, C. H.; Yang, R. X.; Walsh, A.; Kovalenko, M. V. *Nano Lett.* **2015**, *15*, 3692.
(11) Mizusaki, J.; Arai, K.; Fueki, K. *Solid State Ionics* **1983**, *11*, 203.
(12) Akkerman, Q. A.; D'Innocenzo, V.; Accornero, S.; Scarpellini, A.; Petrozza, A.; Prato, M.; Manna, L. *J. Am. Chem. Soc.* **2015**, *137*, 10276.
(13) Nedelcu, G.; Protesescu, L.; Yakunin, S.; Bodnarchuk, M. I.; Grotevent, M. J.; Kovalenko, M. V. *Nano Lett.* **2015**, *15*, 5635.
(14) Song, J.; Li, J.; Li, X.; Xu, L.; Dong, Y.; Zeng, H. *Adv. Mater.* **2015**, *27*, 7162.
(15) Zhang, X.; Lin, H.; Huang, H.; Reckmeier, C.; Zhang, Y.; Choy, W. C. H.; Rogach, A. L. *Nano Lett.* **2016**, *16*, 1415.
(16) Pan, J.; Sarmah, S. P.; Murali, B.; Dursun, I.; Peng, W.; Parida, M. R.; Liu, J.; Sinatra, L.; Alyami, N.; Zhao, C.; Alarousu, E.; Ng, T. K.; Ooi, B. S.; Bakr, O. M.; Mohammed, O. F. *J. Phys. Chem. Lett.* **2015**, *6*, 5027.
(17) Yakunin, S.; Protesescu, L.; Krieg, F.; Bodnarchuk, M. I.; Nedelcu, G.; Humer, M.; De Luca, G.; Fiebig, M.; Heiss, W.; Kovalenko, M. V. *Nat. Commun.* **2015**, *6*, 8056.
(18) Wang, Y.; Li, X.; Zhao, X.; Xiao, L.; Zeng, H.; Sun, H. *Nano Lett.* **2016**, *16*, 448.
(19) Xu, Y.; Chen, Q.; Zhang, C.; Wang, R.; Wu, H.; Zhang, X.; Xing, G.; Yu, W. W.; Wang, X.; Zhang, Y.; Xiao, M. *J. Am. Chem. Soc.* **2016**, *138*, 3761.
(20) Mocatta, D.; Cohen, G.; Schattner, J.; Millo, O.; Rabani, E.; Banin, U. *Science* **2011**, *332*, 77.
(21) Norris, D. J.; Yao, N.; Charnock, F. T.; Kennedy, T. A. *Nano Lett.* **2001**, *1*, 3.
(22) Beaulac, R.; Archer, P. I.; Liu, X.; Lee, S.; Salley, G. M.; Dobrowolska, M.; Furdyna, J. K.; Gamelin, D. R. *Nano Lett.* **2008**, *8*, 1197.
(23) Bussian, D. A.; Crooker, S. A.; Yin, M.; Brynda, M.; Efros, A. L.; Klimov, V. I. *Nat. Mater.* **2009**, *8*, 35.
(24) Beaulac, R.; Schneider, L.; Archer, P. I.; Bacher, G.; Gamelin, D. R. *Science* **2009**, *325*, 973.
(25) Pandey, A.; Brovelli, S.; Viswanatha, R.; Li, L.; Pietryga, J. M.; Klimov, V. I.; Crooker, S. A. *Nat. Nanotechnol.* **2012**, *7*, 792.
(26) Archer, P. I.; Santangelo, S. A.; Gamelin, D. R. *Nano Lett.* **2007**, *7*, 1037.
(27) Rice, W. D.; Liu, W.; Baker, T. A.; Sinitsyn, N. A.; Klimov, V. I.; Crooker, S. A. *Nat. Nanotechnol.* **2016**, *11*, 137.
(28) Pradhan, N.; Goorskey, D.; Thessing, J.; Peng, X. *J. Am. Chem. Soc.* **2005**, *127*, 17586.
(29) Xie, R.; Peng, X. *J. Am. Chem. Soc.* **2009**, *131*, 10645.
(30) Vlaskin, V. A.; Janssen, N.; van Rijssel, J.; Beaulac, R.; Gamelin, D. R. *Nano Lett.* **2010**, *10*, 3670.
(31) McLaurin, E. J.; Vlaskin, V. A.; Gamelin, D. R. *J. Am. Chem. Soc.* **2011**, *133*, 14978.
(32) Bhargava, R. N.; Gallagher, D.; Hong, X.; Nurmikko, A. *Phys. Rev. Lett.* **1994**, *72*, 416.
(33) Chamarro, M.; Voliotis, V.; Grousson, R.; Lavallard, P.; Gacoin, T.; Counio, G.; Boilot, J.; Cases, R. *J. Cryst. Growth* **1996**, *159*, 853.
(34) Vlaskin, V. A.; Barrows, C. J.; Erickson, C. S.; Gamelin, D. R. *J. Am. Chem. Soc.* **2013**, *135*, 14380.
(35) Chamarro, M. A.; Voliotis, V.; Grousson, R.; Lavallard, P.; Gacoin, T.; Counio, G.; Boilot, J. P.; Cases, R. *J. Cryst. Growth* **1996**, *159*, 853.
(36) Counio, G.; Gacoin, T.; Boilot, J. P. *J. Phys. Chem. B* **1998**, *102*, 5257.
(37) Stowell, C. A.; Wiacek, R. J.; Saunders, A. E.; Korgel, B. A. *Nano Lett.* **2003**, *3*, 1441.
(38) Magana, D.; Perera, S. C.; Harter, A. G.; Dalal, N. S.; Strouse, G. F. *J. Am. Chem. Soc.* **2006**, *128*, 2931.
(39) Viswanatha, R.; Brovelli, S.; Pandey, A.; Crooker, S. A.; Klimov, V. I. *Nano Lett.* **2011**, *11*, 4753.
(40) Sahu, A.; Kang, M. S.; Kompch, A.; Notthoff, C.; Wills, A. W.; Deng, D.; Winterer, M.; Frisbie, C. D.; Norris, D. J. *Nano Lett.* **2012**, *12*, 2587.
(41) Hanif, K. M.; Meulenberg, R. W.; Strouse, G. F. *J. Am. Chem. Soc.* **2002**, *124*, 11495.
(42) Archer, P. I.; Santangelo, S. A.; Gamelin, D. R. *J. Am. Chem. Soc.* **2007**, *129*, 9808.
(43) Yang, H.; Holloway, P. H.; Ratna, B. B. *J. Appl. Phys.* **2003**, *93*, 586.
(44) Goede, O.; Heimbrodt, W. *Phys. Status Solidi B* **1988**, *146*, 11.
(45) Bryan, J. D.; Gamelin, D. R. In *Progress in Inorganic Chemistry*; Karlin, K. D., Ed.; John Wiley & Sons, Inc.: New York, 2005; p 47.
(46) Wager, J. F.; Keir, P. D. *Annu. Rev. Mater. Sci.* **1997**, *27*, 223.
(47) Wood, V.; Halpert, J. E.; Panzer, M. J.; Bawendi, M. G.; Bulović, V. *Nano Lett.* **2009**, *9*, 2367.
(48) Bol, A.; Meijerink, A. *Phys. Rev. B: Condens. Matter Mater. Phys.* **1998**, *58*, R15997.
(49) Beaulac, R.; Archer, P. I.; van Rijssel, J.; Meijerink, A.; Gamelin, D. R. *Nano Lett.* **2008**, *8*, 2949.
(50) White, M. A.; Weaver, A. L.; Beaulac, R.; Gamelin, D. R. *ACS Nano* **2011**, *5*, 4158.
(51) Santra, P. K.; Kamat, P. V. *J. Am. Chem. Soc.* **2012**, *134*, 2508.
(52) He, Y.; Wang, H.-F.; Yan, X.-P. *Anal. Chem.* **2008**, *80*, 3832.
(53) Erickson, C. S.; Bradshaw, L. R.; McDowall, S.; Gilbertson, J. D.; Gamelin, D. R.; Patrick, D. L. *ACS Nano* **2014**, *8*, 3461.
(54) Yu, J. H.; Kwon, S.-H.; Petrášek, Z.; Park, O. K.; Jun, S. W.; Shin, K.; Choi, M.; Park, Y. I.; Park, K.; Na, H. B.; Lee, N.; Lee, D. W.; Kim, J. H.; Schwille, P.; Hyeon, T. *Nat. Mater.* **2013**, *12*, 359.
(55) Shannon, R. *Acta Crystallogr., Sect. A: Cryst. Phys., Diffr., Theor. Gen. Crystallogr.* **1976**, *32*, 751.
(56) Moriwaki, M. M.; Becker, W. M.; Gebhardt, W.; Galazka, R. R. *Phys. Rev. B: Condens. Matter Mater. Phys.* **1982**, *26*, 3165.
(57) Erwin, S. C.; Zu, L.; Haftel, M. I.; Efros, A. L.; Kennedy, T. A.; Norris, D. J. *Nature* **2005**, *436*, 91.
(58) Pellet, N.; Teuscher, J.; Maier, J.; Grätzel, M. *Chem. Mater.* **2015**, *27*, 2181.
(59) Bekenstein, Y.; Koscher, B. A.; Eaton, S. W.; Yang, P.; Alivisatos, A. P. *J. Am. Chem. Soc.* **2015**, *137*, 16008.
(60) Ji, T.; Jian, W.-B.; Fang, J. *J. Am. Chem. Soc.* **2003**, *125*, 8448.
(61) Darwent, B. d. *NSRDS-NBS* **1970**, *32*, 79b.
(62) Cottrell, T. L. *Dynamic Aspects of Molecular Energy States*; Wiley: New York, 1965.
(63) Makarov, N. S.; Guo, S.; Isaienko, O.; Liu, W.; Robel, I.; Klimov, V. I. *Nano Lett.* **2016**, *16*, 2349.
(64) Viswanatha, R.; Pietryga, J. M.; Klimov, V. I.; Crooker, S. A. *Phys. Rev. Lett.* **2011**, *107*, 067402.
(65) Dou, L.; Wong, A. B.; Yu, Y.; Lai, M.; Kornienko, N.; Eaton, S. W.; Fu, A.; Bischak, C. G.; Ma, J.; Ding, T.; Ginsberg, N. S.; Wang, L.-W.; Alivisatos, A. P.; Yang, P. *Science* **2015**, *349*, 1518.
(66) Zhang, D.; Eaton, S. W.; Yu, Y.; Dou, L.; Yang, P. *J. Am. Chem. Soc.* **2015**, *137*, 9230.

DOI: 10.1021/jacs.6b08085
J. Am. Chem. Soc. 2016, 138, 14954−14961